

ADVANCED MATERIALS

Supporting Information

for *Adv. Mater.*, DOI: 10.1002/adma.202207635

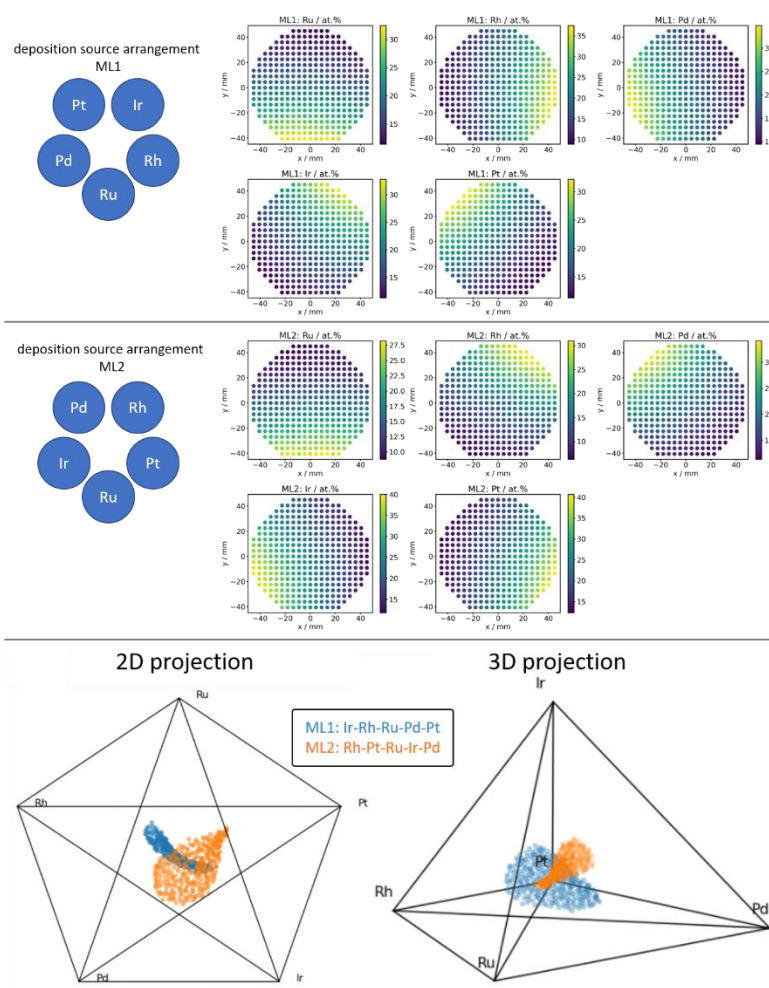
Microscale Combinatorial Libraries for the Discovery of
High-Entropy Materials

*Lars Banko, Emmanuel Batsa Tetteh, Aleksander
Kostka, Tobias Horst Piotrowiak, Olga Anna Krysiak,
Ulrich Hagemann, Corina Andronescu, Wolfgang
Schuhmann,* and Alfred Ludwig**

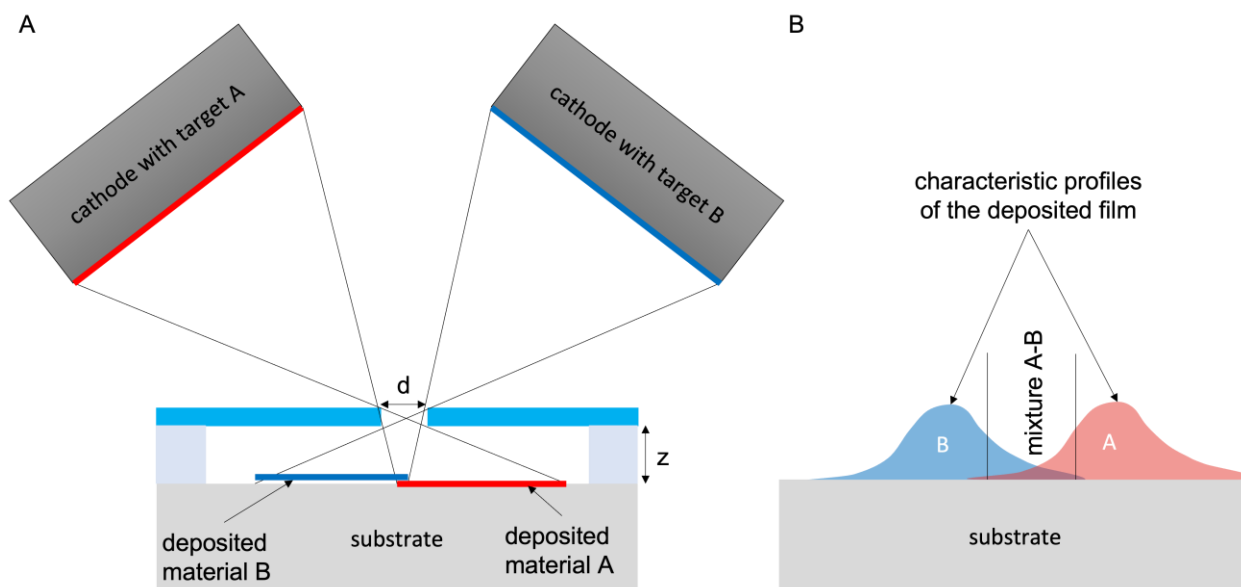
Supporting Information

Microscale combinatorial libraries for the discovery of high entropy materials

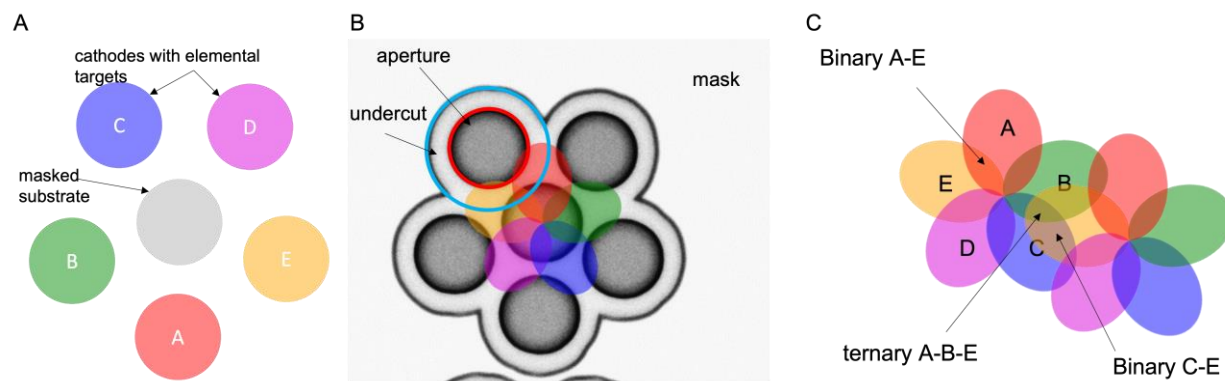
Lars Banko, Emmanuel Batsa Tetteh, Aleksander Kostka, Tobias Horst Piotrowiak, Olga Anna Krysiak, Ulrich Hagemann, Corina Andronescu, Wolfgang Schuhmann*, Alfred Ludwig*



Supplementary Figure 1: Illustration of the effect of deposition source arrangement on the composition gradient of a composition spread materials library. Sputtering from five deposition sources on a planar substrate creates composition gradients of all five elements over the substrate area. This can be seen as creating a two-dimensional plane in a five-dimensional space. As a result, moving from one substrate position to a second substrate position always results in a change of the ratio of all five elements - i.e. there is no set of substrate coordinates for which an individual element concentration is changed while the relative ratios of all other elements are constant. Further, the relative arrangement of the different deposition sources changes the covered composition subspace on the materials library (the two-dimensional plane is located differently in the five-dimensional space). The 2D and 3D projections of the 5D space show how two materials libraries sputtered from different cathode arrangements cut the 5D space.



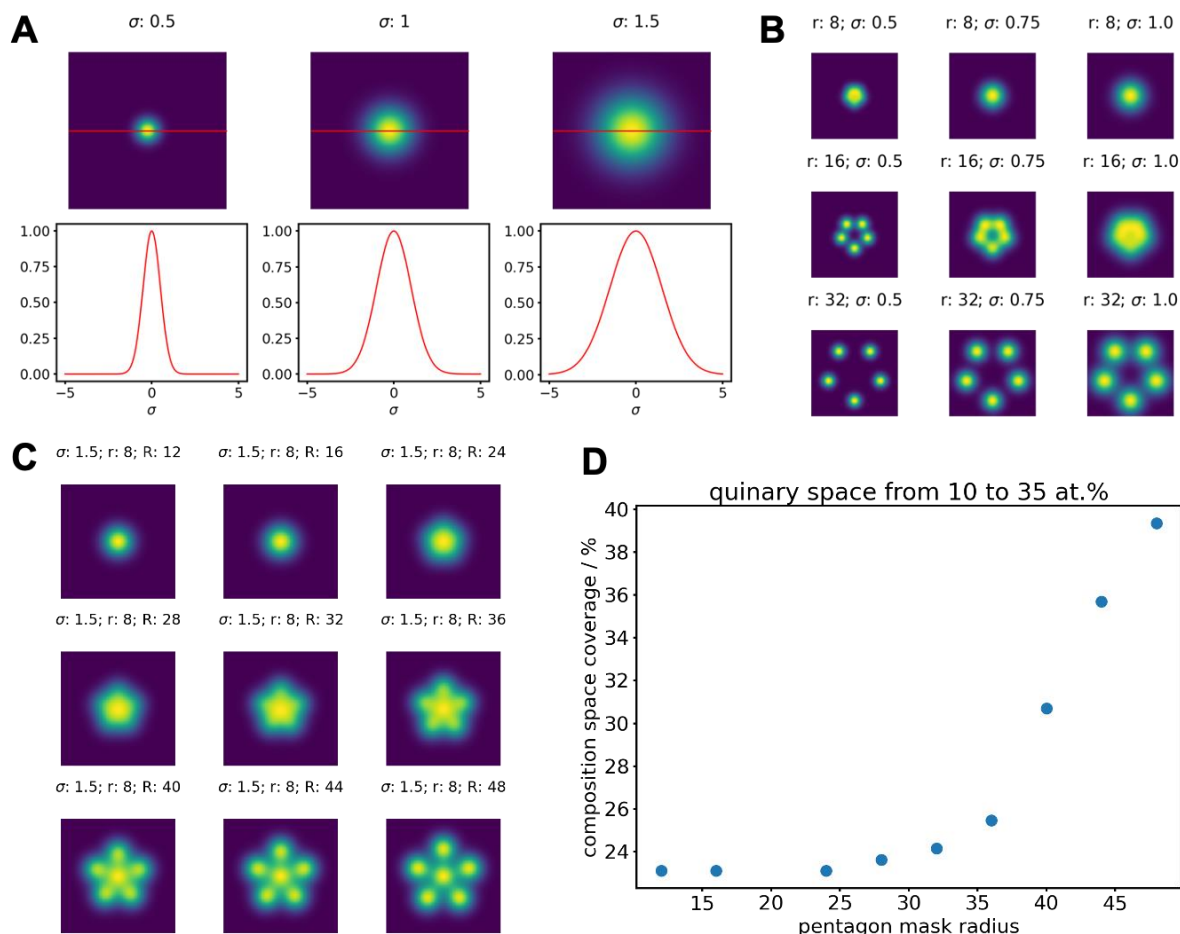
Supplementary Figure 2: (A) Schematic of deposition source arrangement in relation to the masked substrate. The mask is characterized by the aperture diameter d and the mask-to-substrate distance z . (B) Illustration of the resulting deposition profiles after co-deposition from two deposition sources. The region of the binary mixture between the individual elements is indicated in the centre.



Supplementary Figure 3: Illustration of the microlibrary concept. (A) shows the deposition arrangement in top view. Five deposition sources (cathodes) are equipped with elemental targets A-E. The masked substrate is placed in the centre below the deposition sources. (B) shows a microscopy image of the masked substrate. The aperture is indicated by the red circle, 5 μm diameter. The blue circle marks the undercut of the lift-off resist. The coloured shapes illustrate the deposition profiles of the five elements resulting from a deposition through the centre aperture. (C) illustrates the systematic design of composition gradients that result from the relative arrangement of multiple apertures. “Normal” co-deposition from 5 elemental targets would not produce composition with high concentrations of E, B and C (or purely ternary compositions) as the targets are located opposite to each other. Shadow masking using a second aperture in close proximity to the first aperture creates compositions with high concentrations of B, C and E (or the actual ternary composition spread of these elements).

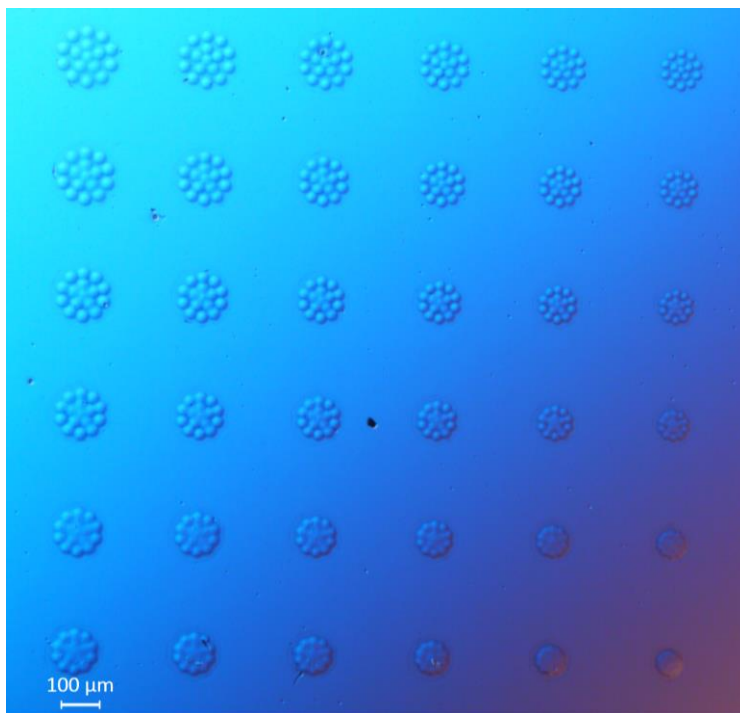
Numerical simulation of composition spreads

The mask design is supported by numerical simulations to estimate the fabricated compositions and the composition space coverage (see Supplementary Figure 4). In the simulation, two-dimensional Gaussian distributions, propagated on a regular grid, are chosen to approximate the deposition profiles from individual elemental sources (see Supplementary Figure 4A). The deposition profiles resulting from co-deposition of five, equidistantly arranged sources through a single aperture are simulated by summing the five 2D Gaussian-profiles that are arranged on a circle with radius r (see Supplementary Figure 4B). The chemical composition is calculated by normalizing the deposition fluxes of the individual elements in each pixel of the simulated substrate grid. The multi-aperture mask is simulated by propagating the deposition profiles on a radius R (Supplementary Figure 4C). The demonstrated design in a pentagon shape is chosen to cover a composition space centred around equiatomic compositions with a variation of each element between 10 and 35 at. %.



Supplementary Figure 4 Simulation of chemical compositions by variation of the mask layout. (A) shows different Gaussian-profiles simulating the thickness profile of material deposited through an aperture. (B) shows deposition profiles resulting from simultaneous co-deposition from five deposition sources through a single aperture. Here, the variation of σ is emulating different deposition profiles of individual elements and r is emulating the ratio of aperture diameter and mask to substrate distance. We evaluated the deposition profiles for a mask design experimentally and observed a profile comparable to $\sigma=1.5$ and $r=8$. (C) shows the superposition of deposition profiles as generated by co-deposition through five apertures arranged on a circle with diameter R around a center aperture, thereby creating overlap between the deposition profiles of single elements. (D) shows the coverage of all possible chemical compositions in a quinary material system in the range from 10 to 35 at.% variation for each element, sampled in 5 at.% steps.

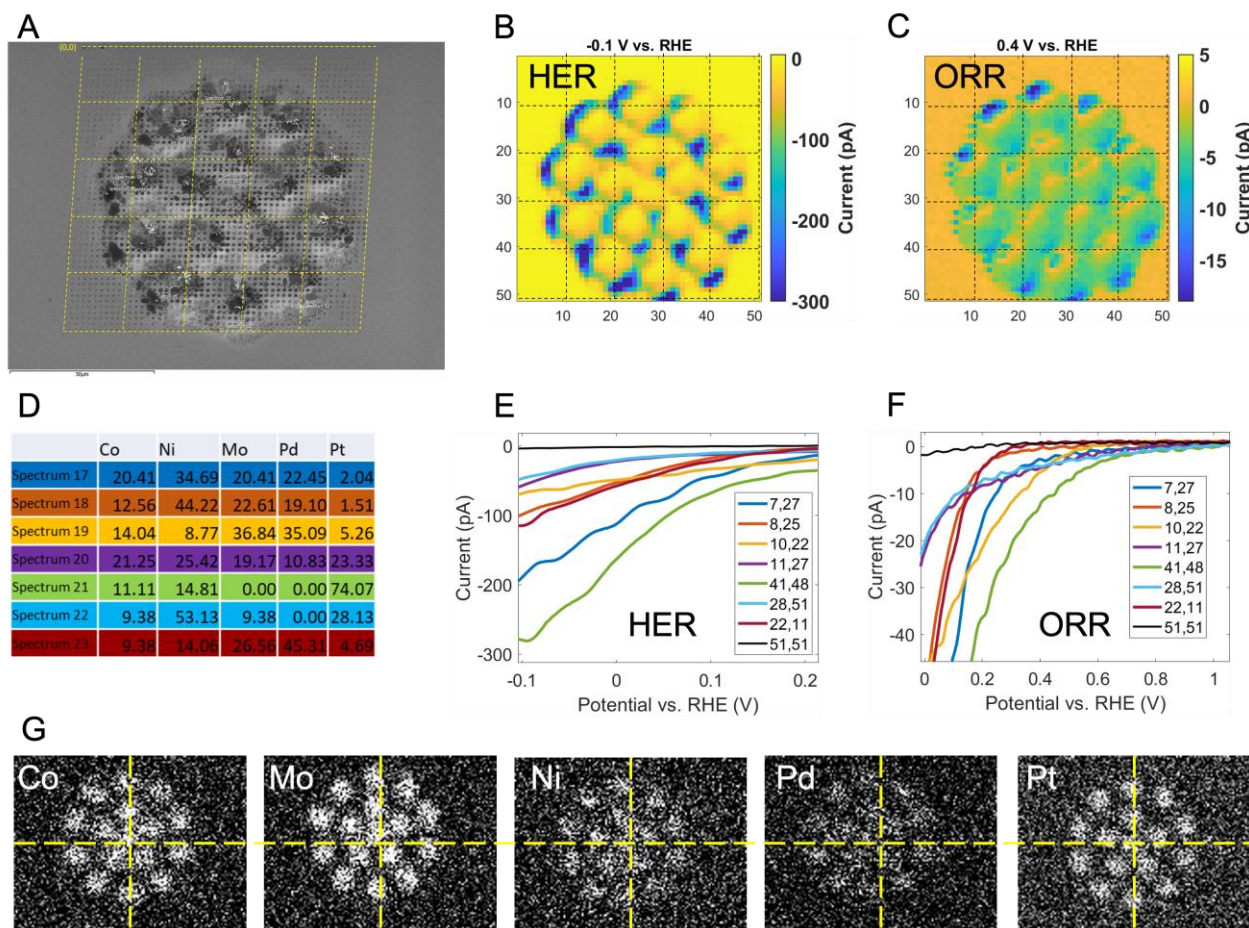
Supplementary Figure 5 illustrates that in principle thousands of microlibraries could be placed on a 100 mm substrate. The mask design of individual libraries could be changed to cover a different section of the total composition space. As such, theoretically the total composition space of multinary systems could be covered in a single deposition process.



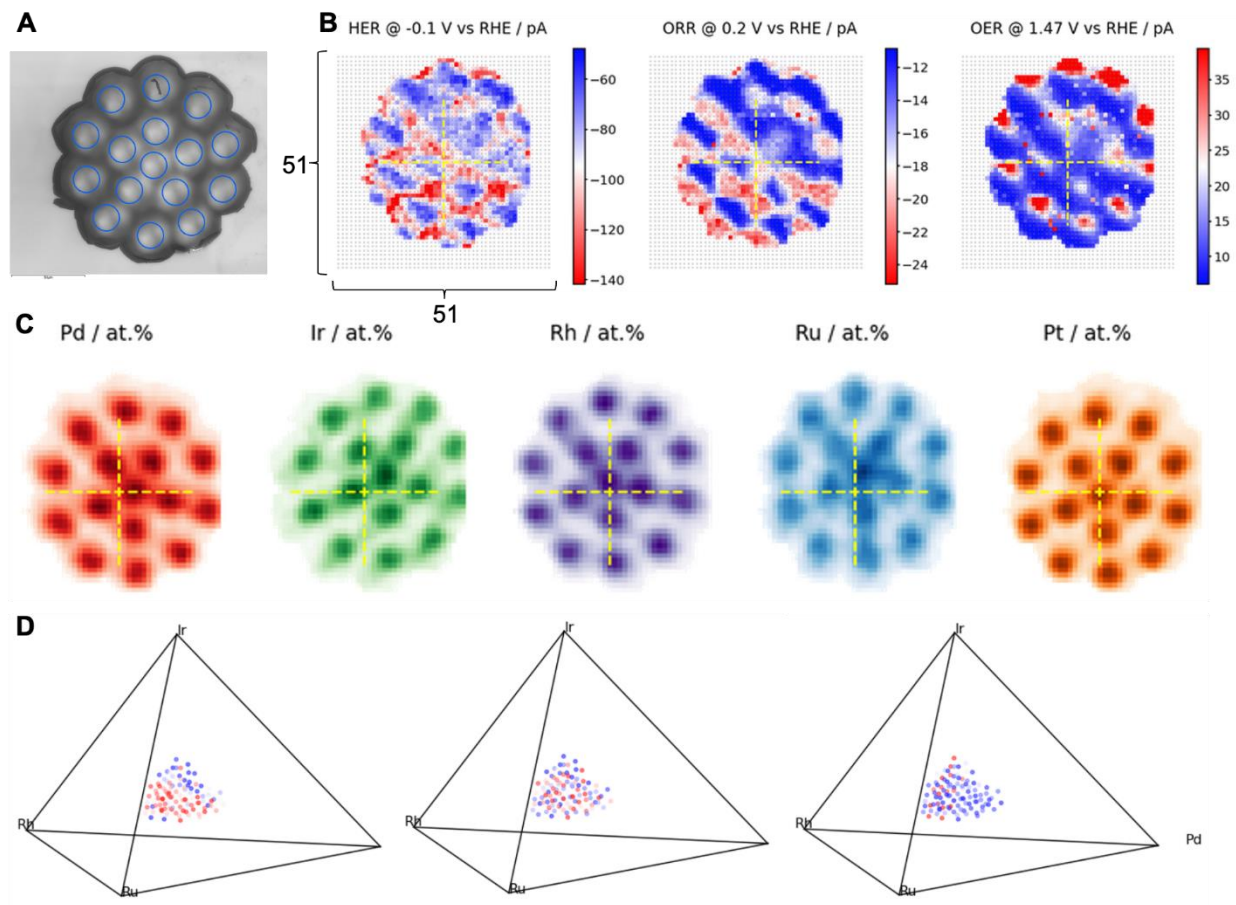
Supplementary Figure 5: Light microscope image showing a set of 36 microlibraries that were deposited through an aperture mask with a variation of aperture diameter and relative distances between apertures.

Screening for noble-metal-lean electrocatalysts

The system Ru-Rh-Pd-Ir-Pt was used as an example to demonstrate the microlibrary concept. We further show that our approach enables the search for noble-metal-lean electrocatalysts by investigating the system Co-Ni-Mo-Pd-Pt for the hydrogen evolution reaction and the oxygen reduction reaction. The substrate was coated by a 20 nm TiN film which provides good electrical conductivity while being electrocatalytically inactive. Supplementary Figure 6A shows an SEM image of the microlibrary after SECCM measurements. The measurement spots from SECCM (51 x 51 spots) are visible as small dots and can be used to select the exact spots for composition measurement with EDX. Supplementary Figure 6B and C show the results of the SECCM measurement for HER and ORR, respectively. Supplementary Figure 6D shows the composition table from individual EDX measurements on selected measurement spots and the corresponding LSV are shown in Supplementary Figure 6E and F for HER and ORR, respectively. The results of the EDX mapping are shown in Supplementary Figure 6G. The most active composition for both HER and ORR is $\text{Co}_{11}\text{Ni}_{15}\text{Mo}_0\text{Pd}_0\text{Pt}_{74}$. The second-best composition for HER is $\text{Co}_{20}\text{Ni}_{35}\text{Mo}_{20}\text{Pd}_{23}\text{Pt}_2$ for which the total noble metal content is only 25 at.%. Similarly, the second-best composition for ORR is $\text{Co}_{14}\text{Ni}_9\text{Mo}_{37}\text{Pd}_{35}\text{Pt}_5$ for which the total noble metal content is reduced to 40 at.%.



Supplementary Figure 6: Results of the exemplary discovery for noble metal lean electrocatalysts. (A) shows an SEM image that was acquired after the SECCM measurement. Residuals of the electrolyte are visible which may be used to guide composition measurement at the exact measurement spot at which the LSV was recorded. (B) and (C) show the activity maps for HER and ORR at -0.1V vs RHE and 0.4 V vs RHE, respectively. (D) shows the EDX measured compositions of the LSV shown in (E) and (F). (G) shows the results of the EDX map of the complete microlibrary for the individual elements.



Supplementary Figure 7: Alternative visualization of the composition and activity of the Pd-Ir-Rh-Ru-Pt microlibrary. A) shows a light microscopy image of the Pd-Ir-Rh-Ru-Pt microlibrary. B) shows electrocatalytic activity maps for HER, ORR and OER. C) shows the chemical composition maps of the microlibrary as acquired by EDX. D) shows the electrocatalytic activity for HER, ORR and OER in a quaternary plot. The composition of Pt was omitted for sake of visualization in quaternary plots.